Search for Post-merger Gravitational Waves from the Remnant of the Binary Neutron Star Merger GW170817

LIGO Scientific Collaboration and Virgo Collaboration
(See the end matter for the full list of authors.)

Abstract

The first observation of a binary neutron star (NS) coalescence by the Advanced LIGO and Advanced Virgo gravitational-wave (GW) detectors offers an unprecedented opportunity to study matter under the most extreme conditions. After such a merger, a compact remnant is left over whose nature depends primarily on the masses of the inspiraling objects and on the equation of state of nuclear matter. This could be either a black hole (BH) or an NS, with the latter being either long-lived or too massive for stability implying delayed collapse to a BH. Here, we present a search for GWs from the remnant of the binary NS merger GW170817 using data from Advanced LIGO and Advanced Virgo. We search for short- ($\lesssim 1$ s) and intermediate-duration ($\lesssim 500$ s) signals, which include GW emission from a hypermassive NS or supramassive NS, respectively. We find no signal from the post-merger remnant. Our derived strain upper limits are more than an order of magnitude larger than those predicted by most models. For short signals, our best upper limit on the root sum square of the GW strain emitted from 1–4 kHz is $h_{\rm rss}^{50\%} = 2.1 \times 10^{-22}$ Hz$^{-1/2}$ at 50% detection efficiency. For intermediate-duration signals, our best upper limit at 50% detection efficiency is $h_{\rm rss}^{50\%} = 8.4 \times 10^{-22}$ Hz$^{-1/2}$ for a millisecond magnetar model, and $h_{\rm rss}^{50\%} = 5.9 \times 10^{-22}$ Hz$^{-1/2}$ for a bar-mode model. These results indicate that post-merger emission from a similar event may be detectable when advanced detectors reach design sensitivity or with next-generation detectors.

Key words: gravitational waves – methods: data analysis – stars: neutron

1. Introduction

On 2017 August 17 12:41:04.4 UTC, the two detectors of the Advanced Laser Interferometer Gravitational-wave Observatory (LIGO) and the Advanced Virgo detector observed GW170817, the gravitational-wave (GW) signal from the coalescence of two compact objects, almost certainly neutron stars (NSs; Abbott et al. 2017a). Supporting this hypothesis were electromagnetic counterparts observed across the spectrum (Abbott et al. 2017b, 2017c). Thanks to its relatively close proximity to Earth, with 90% credible intervals of 40^{+8}_{-14} Mpc as measured by the GW data analysis (Abbott et al. 2017a) and $43.8^{+2.9}_{-6.9}$ Mpc as measured with electromagnetic observations (Abbott et al. 2017d), GW170817 offers the first opportunity to study the nature of the remnant leftover from a binary NS merger using GW observations.

The merger of two NSs can have four possible outcomes: (i) the prompt formation of a black hole (BH), (ii) the formation of a hypermassive NS that collapses to a BH in $\lesssim 1$ s, (iii) the formation of a supramassive NS that collapses to a BH on timescales of ~ 10–10^4 s, or (iv) the formation of a stable NS. The specific outcome of any merger depends on the progenitor masses, with the two NSs that merged in GW170817 having a total mass between 2.73 and 3.29 $M_\odot$ (using the high-spin priors; Abbott et al. 2017a), and also on the NS equation of state (EOS). We present a broad search for both short ($\lesssim 1$ s) and intermediate ($\lesssim 500$ s) duration GW signals potentially emitted from post-merger remnants in scenarios (ii), (iii), and (iv). We find no evidence for a statistically significant signal and set upper limits on possible GW strain amplitudes and GW energy emission.

Before describing the search, we briefly review the four scenarios listed above. If the system promptly forms a BH, the GW quasinormal-mode ringdown signal from a remnant BH in the GW170817 mass range has a dominant frequency around 6 kHz (Shibata & Taniguchi 2006; Baiotti et al. 2008). Current GW detectors are not robustly calibrated at such high frequencies. Moreover, for such a remnant BH the ringdown signal-to-noise ratio at ~ 40 Mpc is vanishingly small. We therefore focus on short- and intermediate-duration GW signals from a possible NS remnant. We also do not target GW emission from a delayed NS-to-BH collapse in scenarios (ii) or (iii) as it is also not likely detectable (e.g., Baiotti et al. 2007).

A hypermassive NS is one that has mass greater than the maximum mass of a uniformly rotating star, but is prevented from collapse through support from differential rotation and thermal gradients (Baumgarte et al. 2000). Rapid cooling through neutrino emission, angular momentum transport associated with magnetic-field effects (such as the magneto-rotational instability and magnetic braking), and the gravitational torque resulting from the non-axisymmetric structure of the merger remnant cause such merger remnants to collapse $\lesssim 1$ s after formation (Shapiro 2000; Hotokezaka et al. 2013). If the star is less massive but still supramassive—i.e., its mass is larger than the maximum for a non-rotating NS—it will spin down through electromagnetic and GW emission, eventually collapsing to a BH between ~ 10 and 5×10^4 s post-merger (Ravi & Lasky 2014).

Taking the posterior distribution for the progenitor masses of GW170817 (Abbott et al. 2017a), one can calculate a probability distribution for the gravitational mass of the post-merger remnant assuming conservation of baryonic mass (and neglecting mass loss to the ejecta). For a broad range of equations of state, this post-merger mass lies in the hypermassive NS regime (see Section 5.2 of Abbott et al. 2017c).

Moreover, observations of a kilonova-like counterpart in the optical and infrared can give insight into the remnant. For

example, observations suggest low-lanthanide ejecta from the merger (Smartt et al. 2017), which may be the result of a hypermassive NS surviving $\gtrsim$100 ms after the merger causing additional neutrino flux over that of prompt BH formation to irradiate the ejecta, increasing the electron fraction and not allowing the formation of lanthanides (Metzger & Fernández 2014; Abbott et al. 2017c, 2017e). However, optical observations at late times also support opacity-heavy models, consistent with a hypermassive NS lifetime <100 ms (Smartt et al. 2017).

A hypermassive NS remnant may also partially explain the delay between the coalescence time of GW170817 and the trigger time of the short γ-ray burst (GRB) 170817A, detected 1.7 s later by the *Fermi* Gamma-ray Burst Monitor (Abbott et al. 2017c; Goldstein et al. 2017).

Simulations of merging binary NSs with hypermassive remnants show that the post-merger GW emission is dominated by the quadrupolar *f*-mode ($\sim$2–4 kHz; Xing et al. 1994; Ruffert et al. 1996; Shibata & Uryū 2000), with broad secondary and tertiary peaks in the $\sim$1.8–4 kHz range (Hotokezaka et al. 2013). Depending on the EOS, the GW signal may include contributions from post-merger emission beginning around 1 kHz (Maione et al. 2017). The structure and locations of the spectral peaks are correlated with the masses and spins of the progenitors (Bernuzzi et al. 2014; Bauswein & Stergioulas 2015; Kastaun & Galeazzi 2015) and the nuclear EOS (Read et al. 2013; Bernuzzi et al. 2015a; Rezzolla & Takami 2016), implying GW observations of a hypermassive NS potentially enable strong constraints on the EOS (Shibata 2005; Bauswein & Janka 2012).

We also consider the scenarios (iii) and (iv) of a longer-lived post-merger remnant. Observations of X-ray afterglows following short GRBs indicate that a fraction of binary NS mergers may result in supramassive or stable NSs lasting $\gg$100 s (e.g., Rowlinson et al. 2013; Lü et al. 2015). GRB 170817A was sub-energetic compared to the population of cosmological short GRBs (Berger 2014; Abbott et al. 2017b; Goldstein et al. 2017), had an atypical X-ray afterglow (Evans et al. 2017; Troja et al. 2017), and had no observations hinting at a central engine remaining active following the GRB emission phase. Nevertheless, no electromagnetic observations rule out a longer-lived post-merger remnant for GW170817.

Gravitational-wave emission mechanisms in this scenario include magnetic-field-induced ellipticities (Bonazzola & Gourgoulhon 1996; Palomba 2001; Cutler 2002), unstable bar modes (Lai & Shapiro 1995; Corsi & Mészáros 2009), and unstable *r*-modes (Andersson 1998; Lindblom et al. 1998). Estimates for the GW amplitude and detectability from such events vary across many orders of magnitude (e.g., Corsi & Mészáros 2009; Fan et al. 2013; Dall'Osso et al. 2015; Doneva et al. 2015; Lasky & Glampedakis 2016; and Section 4).

In summary, electromagnetic observations of this system do not provide definitive evidence for or against any of the four possible post-merger outcomes, motivating this broad search using data-analysis algorithms that are robust to uncertain waveform morphologies. We do not find any candidate post-merger GW signals associated with GW170817. This is not surprising; even considering optimistic models of GW emission from the hypermassive or supramassive NS phases, the signal-to-noise ratio for a post-merger signal from $\sim$40 Mpc in the current LIGO-Virgo network is less than $\sim$1–2 even for a matched-filter search (Takami et al. 2014; Clark et al. 2016).

However, we find that our current GW amplitude sensitivity is within approximately one order of magnitude of theoretical models for post-merger GW emission, implying that, with algorithmic improvements and the LIGO-Virgo network operating at design sensitivity (Abbott et al. 2016a), as well as future detectors, such emission might become detectable.

This Letter is organized as follows. In Section 2, we describe the detectors and data set used. In Section 3, we present the search methods and results for both short- and intermediate-duration GW signals. We discuss the implications and outlook for the future in Section 4.

2. Detectors and Data Quality

The LIGO (Aasi et al. 2015), Virgo (Acernese et al. 2015), and GEO600 (Dooley et al. 2016) detectors were operating at the time of GW170817. The noise amplitude spectral densities are shown in Figure 1, where the general trend of the detectors' sensitivities at high frequencies is due to the reduced interferometer response, interrupted by non-stationary spectral features, many of which have known origins. The noise spectrum of LIGO Hanford is higher than that from Livingston in the frequency band from 100 Hz to 1 kHz; one contribution is correlated laser noise that can be subtracted off-line (Driggers et al. 2017; used, e.g., for the parameter estimation in Abbott et al. 2017a). This search did not make use of such noise subtraction methods. Virgo suffered from large noise fluctuations and non-stationary spectral features at frequencies above 2.5 kHz (Acernese et al. 2015).

Due to a lack of detailed data quality studies available about GEO600, similar to those performed for LIGO and Virgo, data from that detector were not used in this analysis, although the sensitivity to a signal with time and sky location consistent with GW170817 would be roughly equal in Virgo and GEO600. We note, however, that the network signal-to-noise ratio was dominated by the two LIGO detectors.

The algorithm used to search for short-duration signals (Coherent Wave Burst, cWB) used only LIGO data from 1024 to 4096 Hz. Two algorithms were used for intermediate-duration signals: the Stochastic Transient Analysis Multi-detector Pipeline (STAMP) searched from 24 to 2000 Hz and 2000 to 4000 Hz in LIGO-only data, while cWB searches from 24 to 2048 Hz and used LIGO-Virgo data. These algorithms are described in Section 3.

We whitened and removed stationary spectral lines of instrumental origin. Other techniques were employed to minimize the impact of non-stationary spectral features (Abbott et al. 2017e). The data quality of the detectors was checked using the methods applied to previous GW detections (Abbott et al. 2016b). A short-duration instrumental disturbance occurred in the Livingston detector 1.1 s before the coalescence time. Although this transient does not affect the performance of cWB, the STAMP analysis uses data in which the glitch is subtracted from the data (see Figure 2 in Abbott et al. 2017a).

LIGO's calibration uncertainty is 7% in amplitude and 3° in phase below 2 kHz (Abbott et al. 2017a) and 8% in amplitude and 4° in phase above 2 kHz (Cahillane et al. 2017). Virgo's calibration uncertainty is 10% in amplitude and 10° in phase up to 5 kHz (Abbott et al. 2017a). Calibration uncertainties are not taken into account in calculations of upper limits.
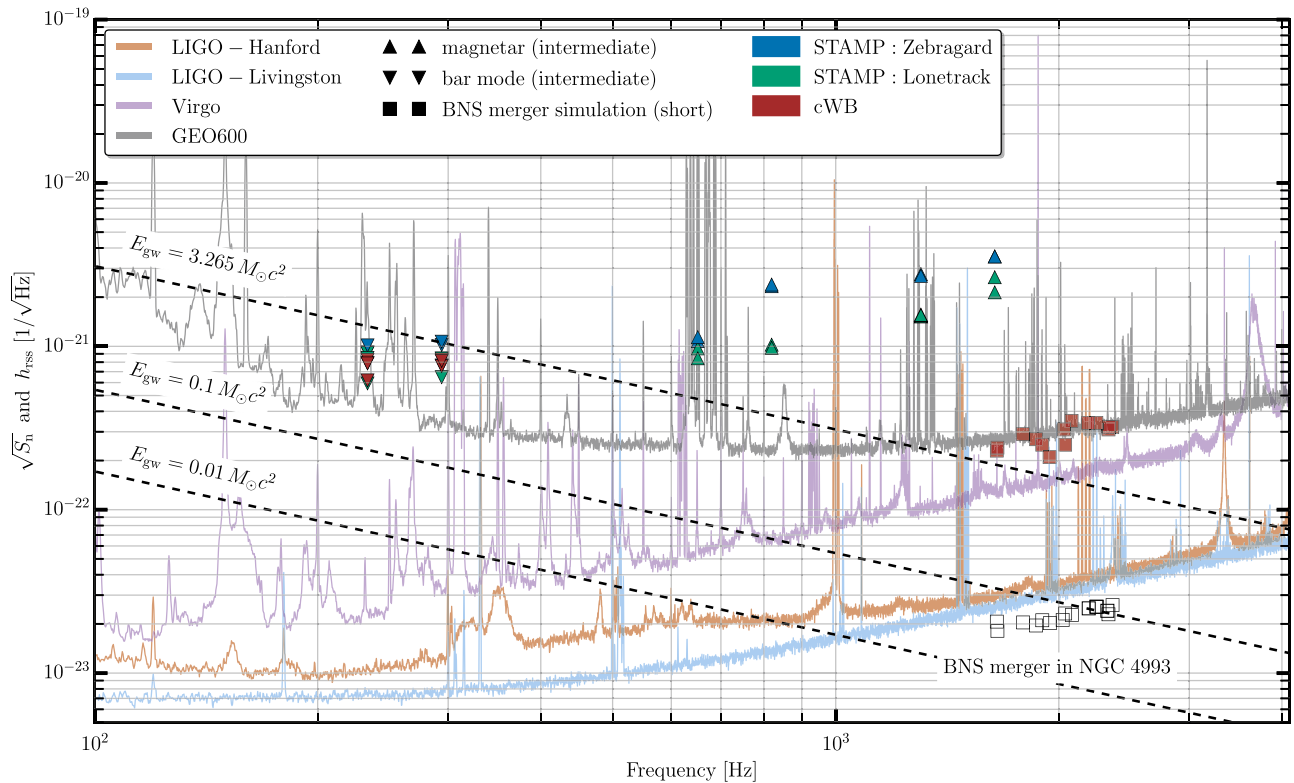
Figure 1. Noise amplitude spectral density $\sqrt{S_n}$ for the four GW detectors (solid curves), and detection efficiency root-sum-square strain amplitudes $h_{\rm rss}$ at 50% false dismissal probability for various waveforms in the short- and intermediate-duration sensitivity studies. The color code of the markers indicates the search, while the marker shapes correspond to the waveform families. The red squares correspond to the short cWB analysis, the red triangles to the intermediate-duration cWB analysis, and the green and blue triangles correspond to the intermediate-duration STAMP Lonetrack and Zebragard analyses, respectively. The frequencies on the x-axis correspond to the average frequency of the injected waveform. The short cWB analysis fixes the polarization to a value consistent with the pre-merger analysis (Abbott et al. 2017a), while for intermediate durations we marginalize over polarization (see the text for details). The top dashed black line indicates the maximum $h_{\rm rss}$ possible for a narrowband GW signal with fixed energy content $E_{\rm gw}$, under the most optimistic assumption that the whole energy available after merger is radiated in GWs at a certain frequency. This energy is obtained from the pre-merger analysis (Abbott et al. 2017a) as $E_{\rm gw} = 3.265\,M_\odot\,c^2$ by subtracting the lower bound of $0.025\,M_\odot\,c^2$ on the radiated energy from the upper end of the 90% credible range on the total system mass. The region above this line can thus be considered an unphysical part of parameter space, and in reality we expect GW emission of only a fraction of this absolute upper bound—as an example, lines at $0.1\,M_\odot\,c^2$ and $0.01\,M_\odot\,c^2$ are also shown. The open squares represent the post-merger NR waveforms used in the short cWB analysis, but at the $h_{\rm rss}$ assuming the distance and orientation of GW170817 inferred from the pre-merger observation in Abbott et al. (2017a). Figure produced using matplotlib (Hunter 2007).

3. Search Methods and Detection Efficiencies

In situations with great theoretical uncertainties, where no complete set of accurate GW template waveforms is available, a matched-filter search is not feasible. Instead, an efficient solution is to search for excess power in spectrograms (also called frequency-time or *ft*-maps) of GW detector data (Anderson et al. 2000; Klimenko & Mitselmakher 2004). Pattern-recognition algorithms are used to identify the presence of GW signals in these maps (Sutton et al. 2010; Thrane et al. 2011; Thrane & Coughlin 2013; Cornish & Littenberg 2015; Klimenko et al. 2016). Here, to account for the large uncertainty in the nature of the remnant, we employ a number of algorithms, each designed to coherently combine data from multiple GW detectors, with different data-processing and clustering techniques that make them respond differently to different waveform models. These algorithms are designed to be sensitive to a wide variety of signal morphologies, and while we test their sensitivity to a number of post-merger waveform models, they are designed so as to be robust against the significant theoretical uncertainties by using generic clustering schemes. Each algorithm performs the search at a single sky position, which we take to be the direction of the host galaxy for the optical counterpart, NGC 4993 (R.A. = 13.1634 hr, decl. = −23°3815; Abbott et al. 2017b; Coulter et al. 2017).

Below, we briefly describe each algorithm used in this search and present their findings.

3.1. Short-duration (≲1 s) Signals

We perform an analysis targeting short-duration, high-frequency GWs near the time of coalescence designed to be sensitive to unmodeled signals. This search for GW bursts is performed using the cWB algorithm (Klimenko et al. 2016). We search for statistically significant coherent excess power due to GW bursts in a 2 s long window that begins at 1187008882 GPS time, includes the estimated time of coalescence, and extends forward in time covering the entire delay between the merger and the GRB (1.7 s; Abbott et al. 2017c).

The cWB algorithm performs a maximum-likelihood evaluation of coherent excess power in a multi-resolution Wilson-Daubechies-Meyer wavelet transform, which is performed on the strain from each detector (Klimenko et al. 2016). The analysis ranks candidate events by their coherent network signal-to-noise ratio. Statistical significance of candidate events is found by comparing the ranking statistic with a background distribution measured from 5.6 days of coincident data from Livingston and Hanford during the period August 13–21. These data are "time-shifted," which means that a non-physical

Table 1
Sensitivity of the cWB Pipeline to Waveforms Generated by Binary NS Simulations

Equation of State	m_1 ($M_\odot$)	m_2 ($M_\odot$)	$\bar{f}$ (Hz)	Simulation	$h_{\rm rss}$ (expected) ($10^{-22}/\sqrt{\rm Hz}$)	$h_{\rm rss}^{50\%}$ ($10^{-22}/\sqrt{\rm Hz}$)
H4 (Glendenning & Moszkowski 1991)	1.25	1.25	1946	Takami et al. (2015)	0.21	2.1
H4 (Glendenning & Moszkowski 1991)	1.3	1.3	2083	Takami et al. (2015)	0.23	3.5
H4 (Glendenning & Moszkowski 1991)	1.35	1.35	2247	Ciolfi et al. (2017)	0.26	3.4
H4 (Glendenning & Moszkowski 1991)	1.42	1.29	2192	Ciolfi et al. (2017)	0.26	3.4
H4 (Glendenning & Moszkowski 1991)	1.54	1.26	2030	Kawamura et al. (2016)	0.22	3.1
LS220 (Lattimer & Swesty 1991)	1.20	1.50	1900	Bauswein et al. (2013a)	0.22	2.5
SHT (Shen et al. 2010)	1.40	1.40	1788	Kastaun et al. (2017)	0.21	2.9
SFHx (Steiner et al. 2013)	1.2	1.5	1650	Bauswein et al. (2013a)	0.21	2.3
SFHx (Steiner et al. 2013)	1.35	1.35	2040	Bauswein et al. (2013a)	0.24	2.5
SLy (Douchin & Haensel 2001)	1.25	1.25	2333	Takami et al. (2015)	0.23	3.2
SLy (Douchin & Haensel 2001)	1.3	1.3	2325	Takami et al. (2015)	0.25	3.1
SLy (Douchin & Haensel 2001)	1.35	1.25	2363	Takami et al. (2015)	0.27	3.2
TMA (Toki et al. 1995)	1.20	1.50	1864	Bauswein et al. (2013a)	0.19	3.2
TMA (Toki et al. 1995)	1.35	1.35	1653	Bauswein et al. (2013a)	0.20	2.4

Note. Waveforms were selected to represent a variety of equations of state (first column) and progenitor mass configurations (second and third columns). The fourth column is the mean frequency for each waveform $\bar{f}$, and the fifth column is the reference for the BNS simulation. The sixth column is the root-sum-squared strain $h_{\rm rss}$ predicted by that simulation for a post-merger signal from a BNS with a distance and inclination consistent with estimates from the inspiral analysis (Abbott et al. 2017a). The seventh column shows the $h_{\rm rss}$ required for 50% detection efficiency with a false-alarm probability of 10^{-4}, $h_{\rm rss}^{50\%}$.

time lag is introduced between the detector analyzed so as to remove correlated GW signals. These data are also "off-source," which means they are outside of the 2 s window over which GWs are searched for. This analysis yields an estimate of the false-alarm probability for a given possible detection.

We search over a frequency range of 1024–4096 Hz. No significant events are found within the 2 s "on-source" window. The sensitivity of the cWB analysis is characterized through Monte Carlo simulations in which waveforms from binary NS post-merger simulations are added to data from off-source periods (see Appendix A.1 for details). The simulated sources are placed at the known sky location of the optical counterpart of GW170817 and with orbital inclination consistent with the pre-merger analysis (Abbott et al. 2017a). The waveform amplitudes are varied to determine the efficiency as a function of signal strength; see B. P. Abbott et al. (2017, in preparation) for an expanded discussion. The response of a given detector to the impinging GW is assumed to take the form

$$s(t) = F_+(\Theta, \psi)h_+(t) + F_\times(\Theta, \psi)h_\times(t), \qquad (1)$$

where F_+ and $F_\times$ are the antenna patterns for a given detector, Θ encodes the direction to the source, and ψ is the polarization angle.

It is customary to express the sensitivity of a search to a given model waveform in $h_{\rm rss}^{50\%}$, which is the root-sum-squared strain amplitude of signals which are detected with 50% efficiency B. P. Abbott et al. (2017, in preparation). The detection criterion has been chosen in this specific search by setting a detection threshold on the significance of candidates which corresponds to a false-alarm probability of 10^{-4}. The quantity $h_{\rm rss}$ is defined as

$$h_{\rm rss} = \sqrt{2 \int_{f_{\rm min}}^{f_{\rm max}} (|\tilde{h}_+(f)|^2 + |\tilde{h}_\times(f)|^2)df}, \qquad (2)$$

where $f_{\rm min}$ and $f_{\rm max}$ are respectively the minimum and maximum frequencies over which the search is performed. The search sensitivities are shown in Figure 1 and Table 1 in terms of the signal-weighted frequency of each waveform, $\bar{f}$,

which describes where the majority of signal power lies in the frequency domain and generally corresponds to the characteristic frequency recovered by the analysis

$$\bar{f} = \frac{2}{h_{\rm rss}^2} \int_{f_{\rm min}}^{f_{\rm max}} df f (|\tilde{h}_+(f)|^2 + |\tilde{h}_\times(f)|^2). \qquad (3)$$

We also provide as a point of comparison the $h_{\rm rss}$ of the same NR waveforms used in the analysis but assuming the distance of GW170817. It is worth noting that softer equation of states (EOSs) that lead to more compact stars exhibit a longer-duration, higher-frequency inspiral phase (Bauswein et al. 2013b) and a more dense remnant with relatively high frequency post-merger oscillations. All NR waveforms have dominant emission well above 1 kHz; however, searching from $f_{\rm min} = 1024$ Hz is a conservative choice made to avoid missing any post-merger-signal content from stiff EOSs but permits pre-merger and merger-signal content from soft EOSs. In the end, the search finds no evidence for any GW signal in this band and the waveforms used to form upper limits are dominated by the post-merger phase, although they do allow for some part of the late inspiral and merger.

The strains required to produce a 50% probability of signal detection lie between 2.1×10^{-22} Hz$^{-1/2}$ and 3.5×10^{-22} Hz$^{-1/2}$. The GW energy radiated by an isotropically emitting source is given by Sutton (2013):

$$E_{\rm gw}^{\rm iso} = \frac{\pi c^3}{2G} \mathcal{D}^2 \int d\Omega \int_{f_{\rm min}}^{f_{\rm max}} df f^2 (|\tilde{h}_+(f)|^2 + |\tilde{h}_\times(f)|^2)$$

$$\approx \frac{\pi^2 c^3}{G} \mathcal{D}^2 \bar{f}^2 h_{\rm rss}^2, \qquad (4)$$

where $\mathcal{D}$ is the distance to the source. Using the $h_{\rm rss}^{50\%}$ sensitivities described above, we find that the energies to which the search is sensitive are 4.8–19.6 $M_\odot c^2$, where the range corresponds to the variety of waveforms used. We are therefore not able to constrain post-merger emission from a possible hypermassive NS associated with GW170817.

A separate analysis of the LIGO-Virgo data for unmodeled short-duration bursts within a $[-600, +60]$ second window around GRB 170817A is reported in Abbott et al. (2017c) using the X-Pipeline package (Sutton et al. 2010; Was et al. 2012). This analysis searched the frequency band of 20–1000 Hz. The inspiral phase of GW170817 was detected with a significance of 4.2σ, rising to 5σ when the analysis is constrained to the optical counterpart location. However, no significant events were found following the merger. Limits on the amplitude of GW emission below 1000 Hz are consistent with those reported here.

3.2. Intermediate-duration ($\lesssim 500\,s$) Signals

For intermediate-duration signals, we employ search algorithms adapted from the all-sky searches described in B. P. Abbott et al. (2017, in preparation). The main difference with respect to the all-sky searches is that instead of searching over many possible sky positions, we again use the known sky position of the optical counterpart. Together with the limited time range to search over, this effectively reduces the number of accidental coincident triggers. Two algorithms are employed: STAMP and cWB.

While the algorithms are sensitive to rather general waveform morphologies, we test the efficiency of signal recovery for both by a set of specific waveform models to determine $h_{\rm rss}^{50\%}$. We coherently add these simulated post-merger signals to the data of LIGO Hanford and Livingston covering the on-source period. The waveforms' polarizations are allowed to vary uniformly in ψ and $\cos\iota$, which corresponds to selecting from an isotropic distribution. The sky positions are fixed to the position of the optical transient. We describe the waveform models in the next section.

3.2.1. Waveform Models

Two types of physically motivated waveform morphologies are considered, corresponding to GWs either from secular bar modes (Lai & Shapiro 1995) or caused by magnetic-field-induced ellipticities of the nascent star (referred to as *magnetar* waveforms in the following; Cutler 2002). Other interesting emission mechanisms are unstable r-modes (Andersson 1998; Mytidis et al. 2015); we do not use such waveforms here due to the duration of their emission, and so searches covering significantly longer timescales will be required.

The secular bar-mode is a GW-driven instability (Chandrasekhar 1970; Friedman & Schutz 1975), where the growth timescale of the mode is determined by the ratio of kinetic to binding energy of the star (Lai & Shapiro 1995). The corresponding waveforms (Corsi & Mészáros 2009) and specific parameters of the model used for the waveforms are given in Appendix A.2 and Table 2.

The magnetar waveforms assume that the merger results in a star that is rapidly spinning down, whose internal magnetic field has been wound up, generating significant stellar ellipticity (e.g., Cutler 2002; Dall'Osso et al. 2009; Ciolfi & Rezzolla 2013). The star then undergoes a spin-flip instability, causing it to become an orthogonal rotator, and hence maximal emitter of GWs. The specific waveform model is derived in Lasky et al. (2017b). The waveform is parameterized by four parameters: a braking index, stellar ellipticity, the initial GW frequency, and the spindown timescale. Details of these waveforms and their parameters are given in Appendix A.3 and Table 3.

Table 2
$h_{\rm rss}$ at 50% Efficiency to the Bar Mode Waveforms Computed for a False-alarm Probability of 10^{-2} for STAMP and 10^{-4} for cWB—See Section 3.2

Properties					$h_{\rm rss}^{50\%}$ ($10^{-22}/\sqrt{\rm Hz}$)		
					cWB	STAMP	
R (km)	B (G)	T (s)	f_0 (Hz)	f_f (Hz)		Lonetrack	Zebragard
12	10^{13}	277	449	139	8.3	8.4	10
12	10^{14}	237	449	139	8.3	9.0	9.2
12	5×10^{14}	107	449	139	7.6	6.5	7.6
14	10^{13}	509	356	111	7.9	8.1	10
14	10^{14}	396	356	111	8.1	8.3	11
14	5×10^{14}	136	356	111	6.2	5.9	7.9

Note. Here, B is the star's dipolar magnetic-field strength at the pole, R the mean stellar radius, T the duration of the waveform in seconds, and f_0 and f_f define the beginning and end of the frequency range where the bulk of the GW energy is emitted. Please see Appendix A.2 for further waveform details.

3.2.2. STAMP

STAMP employs spectrograms with $1\,{\rm s} \times 1\,{\rm Hz}$ pixels created from the cross-correlation of data between spatially separated detectors (Thrane et al. 2011), which in this case are LIGO Hanford and LIGO Livingston. We use 500 s spectrograms covering two frequency bands: 24–2000 Hz and 2000–4000 Hz. The on-source data from the time of merger to the end of the second observing run are split into these 500 s spectrograms with 250 s overlap between them. The time-shifted off-source data are taken from 2017 August 3 until the time of the merger. These are searched with both a seed-based clustering method (Zebragard) and with a seedless pattern-recognition algorithm (Lonetrack) that integrates the pixels across tracks that are picked randomly from a large set of Bézier templates over the spectrogram (Thrane & Coughlin 2013, 2015).

3.2.3. Coherent Wave Burst

For the intermediate-duration search, the cWB algorithm (see Section 3.1 for algorithm details) searches between 24 and 2048 Hz using LIGO-Virgo data from the time of the merger to 1000 s later. Selection criteria for candidate GW triggers are based on the duration of the signal reconstructed by the algorithm as described in B. P. Abbott et al. (2017, in preparation). The on-source time window is taken to be the time of the merger until 1000 s later, while the off-source data are the period from August 13 to 21 with the data time-shifted such that no coherent signals remain.

3.2.4. Results

In the STAMP analysis, the triggers found in the on-source period are compared to the estimated background of accidental coincident triggers; there is no significant excess of coherent events during this time period in the 24–4000 Hz frequency range searched corresponding to a 10^{-2} false-alarm probability. Similarly, no GW transient candidates have been found by cWB above a ranking statistic value corresponding to a 10^{-4} false-alarm probability in the frequency band 24–2048 Hz.

We determine detection efficiencies for the models considered in Section 3.2.1. For STAMP, we report the equivalent energy released at which the algorithms recover 50% or more of the injected signals at a false-alarm probability of 10^{-2}, as well as the

Table 3
h_{rss} at 50% Efficiency to the Magnetar Waveforms Computed for a False-alarm Probability of 10^{-2} for the STAMP Pipelines Used in the Intermediate-duration Search—See Section 3.2

Properties				$h_{\mathrm{rss}}^{50\%}$ $(10^{-22}/\sqrt{\mathrm{Hz}})$	
				STAMP	
ϵ	n	f_0 (Hz)	f_{500} (Hz)	Lonetrack	Zebragard
0.01	2.5	1000	303	9.7	11
0.001	2.5	1000	303	8.4	11
0.01	5	1000	639	10	23
0.001	5	1000	639	9.8	24
0.01	2.5	2000	606	15	28
0.001	2.5	2000	606	16	27
0.01	5	2000	1278	26	35
0.001	5	2000	1278	21	35

Note. The first four columns are respectively the stellar ellipticity ϵ, the braking index n, the initial GW frequency f_0, and the GW frequency after 500 s f_{500}, which is the duration of the analyses. Please see Section A.3 for further waveform details.

corresponding h_{rss}. For cWB, we report the results at a false-alarm probability of 10^{-4}. Due to the rapid rise in background events between false-alarm probabilities of 10^{-2} and 10^{-4}, the results presented here do not depend strongly on this choice. These false-alarm probabilities were chosen as they correspond to a false-alarm rate of approximately 1 per year. The best STAMP results correspond to an $h_{\mathrm{rss}}^{50\%} = 5.9 \times 10^{-22}$ Hz$^{-1/2}$ with an equivalent energy of $E_{\mathrm{GW}} = 2\,M_{\odot}\,c^2$ for the bar-mode signal models. The results for the cWB analysis are similar. For the magnetar signal models, the best STAMP results are $h_{\mathrm{rss}}^{50\%} = 8.4 \times 10^{-22}$ Hz$^{-1/2}$ and $E_{\mathrm{GW}} = 4\,M_{\odot}\,c^2$. cWB did not analyze these waveforms. The energy limits are computed using Equation (4) where isotropic GW emission is assumed and the $h_{\mathrm{rss}}^{50\%}$ values are marginalized over polarization.

4. Implications and Conclusions

We report on a search for GWs from the post-merger remnant following the binary NS coalescence GW170817, using robust and generic time-frequency excess power analysis methods. Such GWs can come from a short-lived hypermassive NS lasting $\lesssim 1$ s before collapsing to a BH or from a longer-lived supramassive or stable NS. We find no evidence in our data for GWs after the merger of GW170817. If a signal exists, it is too weak to be detected with current sensitivity and analysis algorithms.

For the data set and methods employed in this Letter, we find search sensitivities, in terms of GW signal amplitude, that are approximately an order of magnitude from expectations for GW emission in the literature. For example, short-lived hypermassive NSs are expected to emit a few percent of a solar mass in GW energy (e.g., see the two lower dashed lines in Figure 1 that represent 1% and 10% of a solar mass; Kiuchi et al. 2009; Clark et al. 2014; Bernuzzi et al. 2015b; Endrizzi et al. 2016; Dietrich et al. 2017a, 2017b; Feo et al. 2017), while our minimum 50% efficiency is $E_{\mathrm{GW}} \lesssim 4.8\,M_{\odot}\,c^2$ (see Section 3.1). Gravitational-wave emission from a representative sample of these numerical-relativity simulations are shown as open squares in Figure 1, which are approximately an order of magnitude in strain below the $h_{\mathrm{rss}}^{50\%}$ points for the corresponding waveforms (filled squares). For intermediate-duration signals from supramassive or stable NSs (Section 3.2), we find a minimum of $E_{\mathrm{GW}} \lesssim 4\,M_{\odot}\,c^2$ for the

millisecond magnetar model (Lasky et al. 2017b) and $E_{\mathrm{GW}} \lesssim 2\,M_{\odot}\,c^2$ for the model describing secular bar modes (Corsi & Mészáros 2009).

Figure 1 shows the $h_{\mathrm{rss}}^{50\%}$ for the considered waveform models as a function of the waveform's signal-weighted frequency. Based on this, the distance of 40 Mpc for the binary NS is approximately an order of magnitude greater than the distances to which we are sensitive. This gives significant motivation to continue searching for intermediate-duration post-merger remnants in later iterations of the advanced (or future) GW detectors as well as the development of improved analysis methods.

GW170817 was detected in the second observing run of the advanced GW detectors. Further improvements toward their design sensitivity are now underway (Abbott et al. 2016a). At design sensitivity, a matched-filter search with precisely modeled post-merger waveforms could detect signals from a hypermassive NS remnant out to distances of $\sim$20–40 Mpc (computed as the single-detector horizon distance for a signal-to-noise threshold of 5; Takami et al. 2014; Clark et al. 2016). Conversely, with current detector sensitivities and the more robust search methods not relying on matched filtering that are employed in this Letter, a post-merger detection for GW170817 is not very likely a priori, but the theoretical uncertainties still make a search important. By using algorithms designed to be sensitive to generic signals, the searches are robust to these theoretical uncertainties and capable of detection of unmodeled signals.

This study motivates increased research and development toward improved sensitivity at high frequencies in current instruments, planned upgrades and also third-generation interferometers. Future improvements can also be made to the search methods presented in this paper. For example, in searching for short-duration signals, the sparsity of numerical-relativity waveforms makes it challenging to perform matched-filter searches for the inspiral, merger, and hypermassive phases. However, the dominant post-merger GW modes are dictated by only a few pre-merger parameters and the EOS (e.g., Read et al. 2013; Bauswein & Stergioulas 2015; Bernuzzi et al. 2015a; Rezzolla & Takami 2016), implying more sensitive techniques can be developed that use parameters measured during the inspiral to inform priors on the physical parameters of the post-merger remnant.

A full matched-filter search is likely not computationally possible for intermediate-duration signals due to the large parameter spaces and theoretical uncertainties involved with the waveforms. However, sensitivity can be improved by targeting specific emission models (e.g., Coyne et al. 2016).

A search for longer-duration ($\gtrsim 1$ day) remnant signals is also planned, with the maximum detectable signal length limited by the 7.9 days of data available following the merger until the official end of the LIGO-Virgo second observing run. A variant of the intermediate-duration algorithms with different pixel sizes can be used to create spectrograms that cover the full duration of the analysis, making it more sensitive to longer-lived signals than the maps employed here (Thrane et al. 2015). Moreover, a variety of methods have been developed to search for persistent, nearly monochromatic signals from mature NSs (see Prix 2009; Riles 2013; Bejger 2017 for reviews). Several of these could be modified to search for a long-lived post-merger signal, though the expected rapid decrease in frequency is likely to pose technical challenges to current algorithms.

In addition to improving the sensitivity to potential post-merger signals of GW170817, another important program is to improve our ability to detect post-merger GWs from future LIGO-Virgo discoveries of binary NS mergers. At design sensitivity, Advanced LIGO and Advanced Virgo both aim to be approximately a factor of three better in broadband sensitivity than during the second observing run (Abbott et al. 2016a), and next-generation detectors will improve the sensitivities significantly beyond that. This provides a number of opportunities. Clearly, increased sensitivity in the $\gtrsim$kHz range implies improved ability to detect single post-merger signals. Moreover, increased broadband sensitivity implies higher rates of binary NS inspiral and merger detections, and hence might make possible power or coherent stacking of events to increase our sensitivity to post-merger physics (Bose et al. 2017; Yang et al. 2017).

Appendix
Waveforms

Here, we provide details of the waveform models used to determine the detection efficiency of our search algorithms. For short-duration signals (Section 3.1) we use simulations of binary NS mergers. For intermediate durations (Section 3.2.1), we use two models: secular bar modes and magnetar waveforms.

A.1. Binary Neutron Star Waveforms

We determine the efficacy of the short-duration cWB analysis (Section 3.1) through Monte Carlo simulations using GW waveforms derived from simulations of binary NS systems that include a post-merger phase. Table 1 provides a summary of the waveforms in terms of their expected $h_{\rm rss}$ for a binary NS at 40 Mpc and the $h_{\rm rss}$ required for 50% detection efficiency by cWB with a 10^{-4} false-alarm probability, $h_{\rm rss}^{50\%}$. We note that our sample of simulations includes waveforms with relatively stiff EOSs compared with the softer EOSs supported by the pre-merger observations (Abbott et al. 2017a). Post-merger signals from the softer EOSs are likely to be dominated by emission above 2.5 kHz. Including both stiff and soft EOSs is a conservative choice to allow a model-agnostic exploration of the space of waveforms accessible to the unmodeled analysis and demonstrates that the analysis is limited by instrument sensitivity rather than waveform systematics.

A.2. Secular Bar-mode Waveforms

Long-lived post-merger remnants may be unstable due to the secular bar-mode instability. This instability occurs when the ratio of rotational kinetic energy to gravitational binding energy $T/|W|$ is in the range $0.14 < T/|W| < 0.27$ (Lai & Shapiro 1995). For all injected waveforms used in this study we follow the treatment described in Corsi & Mészáros (2009), which we briefly summarize. We set $T/|W| = 0.2$ for the kinetic-to-gravitational potential energy ratio of the initial axisymmetric configuration (in the middle of the secular instability range). The NS spindown is then determined by the combination of magnetic dipole and GW losses (Corsi & Mészáros 2009):

$$\frac{dE}{dt} = -\frac{B^2 R^6 \Omega_{\rm eff}^4}{6c^3} - \frac{32GI^2\epsilon^2\Omega^6}{5c^5}. \quad (5)$$

Here, B is the star's dipolar field strength at the poles, R is the mean stellar radius (i.e., the geometric mean of the principal axes of the star), Ω is the star's angular frequency, $\Omega_{\rm eff}$ is the effective angular frequency (which includes the effect of internal fluid motions), ϵ is the ellipticity, and I is the moment of inertia with respect to the rotation axis. The GW strain is then

$$h(t) = \frac{4G}{c^4}\frac{I\epsilon\,\Omega^2}{\mathcal{D}}, \quad (6)$$

where Ω is found by integrating Equation (5).

For all injected waveforms we assume a total NS mass of 2.6 $M_\odot$, which is close to the lower bound of the estimated total mass range for GW170817 (2.73 $M_\odot$; see Abbott et al. 2017a) and to the lower bound of 2.57 $M_\odot$ for the total mass of other known

binary NS systems (see Abbott et al. 2017a and references therein). For a given initial $T/|W|$ value, the total radiated energy during the secular bar-mode evolution scales as M^2 (see, e.g., Figure 3 in Lai & Shapiro 1995), implying that our value of the mass can be regarded as conservative within the (optimistic) assumption that all of the total mass of the binary goes into the post-merger remnant. We use a range of magnetic-field values from 10^{13} to 5×10^{14} G. Fields higher than $\sim 10^{15}$ G result in rapid spindown of the star, and hence uninteresting GW amplitudes; fields lower than $\sim 10^{13}$ G are unrealistic for such systems given the post-merger remnant dynamics that wind up strong fields. Because we do not know the ultimate fate of the bar-shaped remnant, and whether it can survive up to the ultimate Dedekind configuration (Lai & Shapiro 1995), we only evolve waveforms up to a time when the luminosity emitted in GWs is 1% of the peak value, which is sufficient to capture the bulk of the energy emitted in GWs. Table 2 shows the specific parameters used for our waveforms, as well as h_{rss} at 50% efficiency computed at a fixed false-alarm probability for each of the pipelines used in this search. These results are also shown in Figure 1.

A.3. Magnetar Waveforms

Gravitational waveforms from spinning-down nascent NSs with arbitrary braking index are derived in Lasky et al. (2017b). Here, we assume that the rotational evolution of the star is described by the torque equation: $\dot{\Omega} \propto \Omega^n$, where n is the braking index. Integrating the torque equation enables one to derive the star's spin evolution, and hence the GW frequency

$$ f(t) = f_0 \left(1 + \frac{t}{\tau} \right)^{1/(1-n)}, \tag{7} $$

where f_0 is the initial GW frequency and τ is the spindown timescale. The GW strain is then given by Equation (6), where the GW frequency is twice the star's spin frequency.

A braking index of $n = 5$ represents GW-driven spindown due to stellar ellipticity ϵ, whereas an unchanging dipolar magnetic field in vacuum induces a braking index of $n = 3$. Observations of X-ray afterglows from short GRBs allow for constraints on τ and $\Omega(t = 0)$, and hence f_0 (Rowlinson et al. 2013), as well as ϵ (Lasky & Glampedakis 2016), and n (Lasky et al. 2017a). The braking index of two millisecond magnetars have been measured, both below 3; we therefore choose $n = 2.5$ and $n = 5$ to adequately sample the space. Empirically, such stellar ellipticities are limited to $\lesssim 10^{-2}$, although theoretically such a large value is difficult to generate with internal magnetic fields as it requires a field of $\sim 10^{17}$ G. Large-scale α–Ω dynamos may generate internal fields of $\sim 10^{16}$ G (Thompson & Duncan 1993), with small-scale turbulent dynamos potentially amplifying the field to $\lesssim 5 \times 10^{16}$ G (Zrake & MacFadyen 2013), implying ellipticities as high as $\approx 2.5 \times 10^{-3}$ (Cutler 2002). In principle, the ellipticity should affect the GW frequency evolution; however, in these waveform models that factor is absorbed into τ. Finally, while X-ray observations indicate $10 \lesssim \tau/s \lesssim 10^5$ (Rowlinson et al. 2013), we only show waveform results here using $\tau = 100$ s as larger τ yields uninteresting GW limits.

Table 3 shows waveform parameters used in this study and corresponding h_{rss} at 50% efficiency computed for a fixed false-alarm probability of 10^{-2}. We do not list the duration of

the waveform as all magnetar waveforms are longer than the search duration.

References

Aasi, J., Abbott, B. P., Abbott, R., et al. 2015, CQGra, 32, 074001
Abbott, B. P., Abbott, R., Abbott, T. D., et al. 2016a, LRR, 19, 1
Abbott, B. P., Abbott, R., Abbott, T. D., et al. 2016b, CQGra, 33, 134001
Abbott, B. P., Abbott, R., Abbott, T. D., et al. 2017a, PhRvL, 119, 161101
Abbott, B. P., Abbott, R., Abbott, T. D., et al. 2017b, ApJL, 848, L12
Abbott, B. P., Abbott, R., Abbott, T. D., et al. 2017c, ApJL, 848, L13
Abbott, B. P., Abbott, R., Abbott, T. D., et al. 2017d, Natur, 551, 85
Abbott, B. P., Abbott, R., Abbott, T. D., et al. 2017e, ApJL, 850, L39
Acernese, F., Agathos, M., Agatsuma, K., et al. 2015, CQGra, 32, 024001
Anderson, W. G., Brady, P. R., Creighton, J. D. E., & Flanagan, E. E. 2000, IJMPD, 9, 303
Andersson, N. 1998, ApJ, 502, 708
Baiotti, L., Giacomazzo, B., & Rezzolla, L. 2008, PhRvD, 78, 084033
Baiotti, L., Hawke, I., & Rezzolla, L. 2007, CQGra, 24, S187
Baumgarte, T. W., Shapiro, S. L., & Shibata, M. 2000, ApJL, 528, L29
Bauswein, A., Baumgarte, T. W., & Janka, H.-T. 2013a, PhRvL, 111, 131101
Bauswein, A., Goriely, S., & Janka, H.-T. 2013b, ApJ, 773, 78
Bauswein, A., & Janka, H. T. 2012, PhRvL, 108, 011101
Bauswein, A., & Stergioulas, N. 2015, PhRvD, 91, 124056
Bejger, M. 2017, arXiv:1710.06607
Berger, E. 2014, ARA&A, 52, 43
Bernuzzi, S., Dietrich, T., & Nagar, A. 2015a, PhRvL, 115, 091101
Bernuzzi, S., Nagar, A., Balmelli, S., Dietrich, T., & Ujevic, M. 2014, PhRvL, 112, 201101
Bernuzzi, S., Nagar, A., Dietrich, T., & Damour, T. 2015b, PhRvL, 114, 161103
Bonazzola, S., & Gourgoulhon, E. 1996, A&A, 312, 675
Bose, S., Chakravarti, K., Rezzolla, L., Sathyaprakash, B. S., & Takami, K. 2017, arXiv:1705.10850
Cahillane, C., Betzwieser, J., Brown, D. A., et al. 2017, PhRvD, 96, 102001
Chandrasekhar, S. 1970, PhRvL, 24, 611
Ciolfi, R., Kastaun, W., Giacomazzo, B., et al. 2017, PhRvD, 95, 063016
Ciolfi, R., & Rezzolla, L. 2013, MNRAS, 435, L43
Clark, J., Bauswein, A., Cadonati, L., et al. 2014, PhRvD, 90, 062004
Clark, J. A., Bauswein, A., Stergioulas, N., & Shoemaker, D. 2016, CQGra, 33, 085003
Cornish, N. J., & Littenberg, T. B. 2015, CQGra, 32, 135012
Corsi, A., & Mészáros, P. 2009, ApJ, 702, 1171
Coulter, D. A., Foley, R. J., Kilpatrick, C. D., et al. 2017, Sci, https://doi.org/10.1126/science.aap9811
Coyne, R., Corsi, A., & Owen, B. J. 2016, PhRvD, 93, 104059
Cutler, C. 2002, PhRvD, 66, 084025
Dall'Osso, S., Giacomazzo, B., Perna, R., & Stella, L. 2015, ApJ, 798, 25
Dall'Osso, S., Shore, S. N., & Stella, L. 2009, MNRAS, 398, 1869
Dietrich, T., Bernuzzi, S., Ujevic, M., & Tichy, W. 2017a, PhRvD, 95, 044045
Dietrich, T., Ujevic, M., Tichy, W., Bernuzzi, S., & Brügmann, B. 2017b, PhRvD, 95, 024029
Doneva, D. D., Kokkotas, K. D., & Pnigouras, P. 2015, PhRvD, 92, 104040
Dooley, K. L., Leong, J. R., Adams, T., et al. 2016, CQGra, 33, 075009
Douchin, F., & Haensel, P. 2001, A&A, 380, 151
Driggers, J. C., Vitalie, S., Lundgren, A., et al. 2017, Offline Noise Subtraction for Advanced LIGO, Tech. Rep. LIGO-P1700260, https://dcc.ligo.org/P1700260/public
Endrizzi, A., Ciolfi, R., Giacomazzo, B., Kastaun, W., & Kawamura, T. 2016, CQGra, 33, 164001
Evans, P., Cenko, S. B., Kennea, J. A., et al. 2017, Sci, https://doi.org/10.1126/science.aap9580
Fan, Y.-Z., Wu, X.-F., & Wei, D.-M. 2013, PhRvD, 88, 067304
Feo, A., De Pietri, R., Maione, F., & Löffler, F. 2017, CQGra, 34, 034001
Friedman, J. L., & Schutz, B. F. 1975, ApJL, 199, L157
Glendenning, N. K., & Moszkowski, S. A. 1991, PhRvL, 67, 2414
Goldstein, A., Veres, P., Burns, E., et al. 2017, ApJL, 848, L14
Hotokezaka, K., Kiuchi, K., Kyutoku, K., et al. 2013, PhRvD, 88, 044026
Hunter, J. D. 2007, CSE, 9, 90
Kastaun, W., Ciolfi, R., Endrizzi, A., & Giacomazzo, B. 2017, PhRvD, 96, 043019
Kastaun, W., & Galeazzi, F. 2015, PhRvD, 91, 064027
Kawamura, T., Giacomazzo, B., Kastaun, W., et al. 2016, PhRvD, 94, 064012
Kiuchi, K., Sekiguchi, Y., Shibata, M., & Taniguchi, K. 2009, PhRvD, 80, 064037

Klimenko, S., & Mitselmakher, G. 2004, CQGra, 21, S1819
Klimenko, S., Vedovato, G., Drago, M., et al. 2016, PhRvD, 93, 042004
Lai, D., & Shapiro, S. L. 1995, ApJ, 442, 259
Lasky, P. D., & Glampedakis, K. 2016, MNRAS, 458, 1660
Lasky, P. D., Leris, C., Rowlinson, A., & Glampedakis, K. 2017a, ApJL, 843, L1
Lasky, P. D., Sarin, N., & Sammut, L. 2017b, Long-duration Waveform Models for Millisecond Magnetars Born in Binary Neutron Star Mergers, Tech. Rep. LIGO-T1700408, https://dcc.ligo.org/LIGO-T1700408/public
Lattimer, J. M., & Swesty, F. D. 1991, NuPhA, 535, 331
Lindblom, L., Owen, B. J., & Morsink, S. M. 1998, PhRvL, 80, 4843
Lü, H.-J., Zhang, B., Lei, W.-H., Li, Y., & Lasky, P. D. 2015, ApJ, 805, 89
Maione, F., De Pietri, R., Feo, A., & Löffler, F. 2017, PhRvD, 96, 063011
Metzger, B. D., & Fernández, R. 2014, MNRAS, 441, 3444
Mytidis, A., Coughlin, M., & Whiting, B. 2015, ApJ, 810, 27
Palomba, C. 2001, A&A, 367, 525
Prix, R. 2009, in Gravitational Waves from Spinning Neutron Stars, ed. W. Becker (Berlin: Springer), 651
Ravi, V., & Lasky, P. D. 2014, MNRAS, 441, 2433
Read, J. S., Baiotti, L., Creighton, J. D. E., et al. 2013, PhRvD, 88, 044042
Rezzolla, L., & Takami, K. 2016, PhRvD, 93, 124051
Riles, K. 2013, PrPNP, 68, 1
Rowlinson, A., O'Brien, P. T., Metzger, B. D., Tanvir, N. R., & Levan, A. J. 2013, MNRAS, 430, 1061
Ruffert, M., Janka, H.-T., & Schaefer, G. 1996, A&A, 311, 532

Shapiro, S. L. 2000, ApJ, 544, 397
Shen, G., Horowitz, C. J., & Teige, S. 2010, PhRvC, 82, 015806
Shibata, M. 2005, PhRvL, 94, 201101
Shibata, M., & Taniguchi, K. 2006, PhRvD, 73, 064027
Shibata, M., & Uryū, K. B. O. 2000, PhRvD, 61, 064001
Smartt, S. J., Chen, T. W., Jerkstrand, A., et al. 2017, Natur, 551, 75
Steiner, A. W., Hempel, M., & Fischer, T. 2013, ApJ, 774, 17
Sutton, P. J. 2013, arXiv:1304.0210
Sutton, P. J., Jones, G., Chatterji, S., et al. 2010, NJPh, 12, 053034
Takami, K., Rezzolla, L., & Baiotti, L. 2014, PhRvL, 113, 091104
Takami, K., Rezzolla, L., & Baiotti, L. 2015, PhRvD, 91, 064001
Thompson, C., & Duncan, R. C. 1993, ApJ, 408, 194
Thrane, E., & Coughlin, M. 2013, PhRvD, 88, 083010
Thrane, E., & Coughlin, M. 2015, PhRvL, 115, 181102
Thrane, E., Kandhasamy, S., Ott, C. D., et al. 2011, PhRvD, 83, 083004
Thrane, E., Mandic, V., & Christensen, N. 2015, PhRvD, 91, 104021
Toki, H., Hirata, D., Sugahara, Y., Sumiyoshi, K., & Tanihata, I. 1995, NuPhA, 588, 357
Troja, E., Piro, L., van Eerten, H., et al. 2017, Natur, 551, 74
Was, M., Sutton, P. J., Jones, G., & Leonor, I. 2012, PhRvD, 86, 022003
Xing, Z.-G., Centrella, J. M., & McMillan, S. L. W. 1994, PhRvD, 50, 6247
Yang, H., Paschalidis, V., Yagi, K., et al. 2017, arXiv:1707.00207
Zrake, J., & MacFadyen, A. I. 2013, ApJL, 769, L29

B. P. Abbott[1], R. Abbott[1], T. D. Abbott[2], F. Acernese[3,4], K. Ackley[5,6], C. Adams[7], T. Adams[8], P. Addesso[9], R. X. Adhikari[1], V. B. Adya[10], C. Affeldt[10], M. Afrough[11], B. Agarwal[12], M. Agathos[13], K. Agatsuma[14], N. Aggarwal[15], O. D. Aguiar[16], L. Aiello[17,18], A. Ain[19], P. Ajith[20], B. Allen[10,21,22], G. Allen[12], A. Allocca[23,24], P. A. Altin[25], A. Amato[26], A. Ananyeva[1], S. B. Anderson[1], W. G. Anderson[21], S. V. Angelova[27], S. Antier[28], S. Appert[1], K. Arai[1], M. C. Araya[1], J. S. Areeda[29], N. Arnaud[28,30], K. G. Arun[31], S. Ascenzi[32,33], G. Ashton[10], M. Ast[34], S. M. Aston[7], P. Astone[35], D. V. Atallah[36], P. Aufmuth[22], C. Aulbert[10], K. AultONeal[37], C. Austin[2], A. Avila-Alvarez[29], S. Babak[38], P. Bacon[39], M. K. M. Bader[14], S. Bae[40], P. T. Baker[41], F. Baldaccini[42,43], G. Ballardin[30], S. W. Ballmer[44], S. Banagiri[45], J. C. Barayoga[1], S. E. Barclay[46], B. C. Barish[1], D. Barker[47], K. Barkett[48], F. Barone[3,4], B. Barr[46], L. Barsotti[15], M. Barsuglia[39], D. Barta[49], J. Bartlett[47], I. Bartos[5,50], R. Bassiri[51], A. Basti[23,24], J. C. Batch[47], M. Bawaj[43,52], J. C. Bayley[46], M. Bazzan[53,54], B. Bécsy[55], C. Beer[10], M. Bejger[56], I. Belahcene[28], A. S. Bell[46], B. K. Berger[1], G. Bergmann[10], S. Bernuzzi[57,58], J. J. Bero[59], C. P. L. Berry[60], D. Bersanetti[61], A. Bertolini[14], J. Betzwieser[7], S. Bhagwat[44], R. Bhandare[62], I. A. Bilenko[63], G. Billingsley[1], C. R. Billman[5], J. Birch[7], R. Birney[64], O. Birnholtz[10], S. Biscans[1,15], S. Biscoveanu[6,65], A. Bisht[22], M. Bitossi[24,30], C. Biwer[44], M. A. Bizouard[28], J. K. Blackburn[1], J. Blackman[48], C. D. Blair[1,66], D. G. Blair[66], R. M. Blair[47], S. Bloemen[67], O. Bock[10], N. Bode[10], M. Boer[68], G. Bogaert[68], A. Bohe[38], F. Bondu[69], E. Bonilla[51], R. Bonnand[8], B. A. Boom[14], R. Bork[1], V. Boschi[24,30], S. Bose[19,70], K. Bossie[7], Y. Bouffanais[39], A. Bozzi[30], C. Bradaschia[24], P. R. Brady[21], M. Branchesi[17,18], J. E. Brau[71], T. Briant[72], A. Brillet[68], M. Brinkmann[10], V. Brisson[28], P. Brockill[21], J. E. Broida[73], A. F. Brooks[1], D. A. Brown[44], D. D. Brown[74], S. Brunett[1], C. C. Buchanan[2], A. Buikema[15], T. Bulik[75], H. J. Bulten[14,76], A. Buonanno[38,77], D. Buskulic[8], C. Buy[39], R. L. Byer[51], M. Cabero[10], L. Cadonati[78], G. Cagnoli[26,79], C. Cahillane[1], J. Calderón Bustillo[78], T. A. Callister[1], E. Calloni[4,80], J. B. Camp[81], M. Canepa[61,82], P. Canizares[67], K. C. Cannon[83], H. Cao[74], J. Cao[84], C. D. Capano[10], E. Capocasa[39], F. Carbognani[30], S. Caride[85], M. F. Carney[86], J. Casanueva Diaz[28], C. Casentini[32,33], S. Caudill[14,21], M. Cavaglià[11], F. Cavalier[28], R. Cavalieri[30], G. Cella[24], C. B. Cepeda[1], P. Cerdá-Durán[87], G. Cerretani[23,24], E. Cesarini[33,88], S. J. Chamberlin[65], M. Chan[46], S. Chao[89], P. Charlton[90], E. Chase[91], E. Chassande-Mottin[39], D. Chatterjee[21], B. D. Cheeseboro[41], H. Y. Chen[92], X. Chen[66], Y. Chen[48], H.-P. Cheng[5], H. Chia[5], A. Chincarini[61], A. Chiummo[30], T. Chmiel[86], H. S. Cho[93], M. Cho[77], J. H. Chow[25], N. Christensen[68,73], Q. Chu[66], A. J. K. Chua[13], S. Chua[72], A. K. W. Chung[94], S. Chung[66], G. Ciani[5,53,54], R. Ciolfi[95,96], C. E. Cirelli[51], A. Cirone[61,82], F. Clara[47], J. A. Clark[78], P. Clearwater[97], F. Cleva[68], C. Cocchieri[11], E. Coccia[17,18], P.-F. Cohadon[72], D. Cohen[28], A. Colla[35,98], C. G. Collette[99], L. R. Cominsky[100], M. Constancio, Jr.[16], L. Conti[54], S. J. Cooper[60], P. Corban[7], T. R. Corbitt[2], I. Cordero-Carrión[101], K. R. Corley[50], A. Corsi[85], S. Cortese[30], C. A. Costa[16], M. W. Coughlin[1,73], S. B. Coughlin[91], J.-P. Coulon[68], S. T. Countryman[50], P. Couvares[1], P. B. Covas[102], E. E. Cowan[78], D. M. Coward[66], M. J. Cowart[7], D. C. Coyne[1], R. Coyne[85], J. D. E. Creighton[21], T. D. Creighton[103], J. Cripe[2], S. G. Crowder[104], T. J. Cullen[2,29], A. Cumming[46], L. Cunningham[46], E. Cuoco[30], T. Dal Canton[81], G. Dálya[55], S. L. Danilishin[10,22], S. D'Antonio[33], K. Danzmann[10,22], A. Dasgupta[105], C. F. Da Silva Costa[5], V. Dattilo[30], I. Dave[62], M. Davier[28], D. Davis[44], E. J. Daw[106], B. Day[78], S. De[44], D. DeBra[51], J. Degallaix[26], M. De Laurentis[4,17], S. Deléglise[72], W. Del Pozzo[23,24,60], N. Demos[15], T. Denker[10], T. Dent[10], R. De Pietri[57,58], V. Dergachev[38], R. De Rosa[4,80], R. T. DeRosa[7], C. De Rossi[26,30], R. DeSalvo[107], O. de Varona[10], J. Devenson[27], S. Dhurandhar[19], M. C. Díaz[103], T. Dietrich[38], L. Di Fiore[4], M. Di Giovanni[96,108], T. Di Girolamo[4,50,80], A. Di Lieto[23,24], S. Di Pace[35,98], I. Di Palma[35,98], F. Di Renzo[23,24], Z. Doctor[92], V. Dolique[26], F. Donovan[15], K. L. Dooley[11], S. Doravari[10],

I. Dorrington[36], R. Douglas[46], M. Dovale Álvarez[60], T. P. Downes[21], M. Drago[10], C. Dreissigacker[10], J. C. Driggers[47], Z. Du[84], M. Ducrot[8], P. Dupej[46], S. E. Dwyer[47], T. B. Edo[106], M. C. Edwards[73], A. Effler[7], H.-B. Eggenstein[10,38], P. Ehrens[1], J. Eichholz[1], S. S. Eikenberry[5], R. A. Eisenstein[15], R. C. Essick[15], D. Estevez[8], Z. B. Etienne[41], T. Etzel[1], M. Evans[15], T. M. Evans[7], M. Factourovich[50], V. Fafone[17,32,33], H. Fair[44], S. Fairhurst[36], X. Fan[84], S. Farinon[61], B. Farr[92], W. M. Farr[60], E. J. Fauchon-Jones[36], M. Favata[109], M. Fays[36], C. Fee[86], H. Fehrmann[10], J. Feicht[1], M. M. Fejer[51], A. Fernandez-Galiana[15], I. Ferrante[23,24], E. C. Ferreira[16], F. Ferrini[30], F. Fidecaro[23,24], D. Finstad[44], I. Fiori[30], D. Fiorucci[39], M. Fishbach[92], R. P. Fisher[44], M. Fitz-Axen[45], R. Flaminio[26,110], M. Fletcher[46], E. Flynn[29], H. Fong[111], J. A. Font[87,112], P. W. F. Forsyth[25], S. S. Forsyth[78], J.-D. Fournier[68], S. Frasca[35,98], F. Frasconi[24], Z. Frei[55], A. Freise[60], R. Frey[71], V. Frey[28], E. M. Fries[1], P. Fritschel[15], V. V. Frolov[7], P. Fulda[5], M. Fyffe[7], H. Gabbard[46], B. U. Gadre[19], S. M. Gaebel[60], J. R. Gair[113], L. Gammaitoni[42], M. R. Ganija[74], S. G. Gaonkar[19], C. Garcia-Quiros[102], F. Garufi[4,80], B. Gateley[47], S. Gaudio[37], G. Gaur[114], V. Gayathri[115], N. Gehrels[81,161], G. Gemme[61], E. Genin[30], A. Gennai[24], D. George[12], J. George[62], L. Gergely[116], V. Germain[8], S. Ghonge[78], Abhirup Ghosh[20], Archisman Ghosh[14,20], S. Ghosh[14,21,67], J. A. Giaime[2,7], K. D. Giardina[7], A. Giazotto[24], K. Gill[37], L. Glover[107], E. Goetz[117], R. Goetz[5], S. Gomes[36], B. Goncharov[6], G. González[2], J. M. Gonzalez Castro[23,24], A. Gopakumar[118], M. L. Gorodetsky[63], S. E. Gossan[1], M. Gosselin[30], R. Gouaty[8], A. Grado[4,119], C. Graef[46], M. Granata[26], A. Grant[46], S. Gras[15], C. Gray[47], G. Greco[120,121], A. C. Green[60], E. M. Gretarsson[37], P. Groot[67], H. Grote[10], S. Grunewald[38], P. Gruning[28], G. M. Guidi[120,121], X. Guo[84], A. Gupta[65], M. K. Gupta[105], K. E. Gushwa[1], E. K. Gustafson[1], R. Gustafson[117], O. Halim[17,18], B. R. Hall[70], E. D. Hall[15], E. Z. Hamilton[36], G. Hammond[46], M. Haney[122], M. M. Hanke[10], J. Hanks[47], C. Hanna[65], M. D. Hannam[36], O. A. Hannuksela[94], J. Hanson[7], T. Hardwick[2], J. Harms[17,18], G. M. Harry[123], I. W. Harry[38], M. J. Hart[46], C.-J. Haster[111], K. Haughian[46], J. Healy[59], A. Heidmann[72], M. C. Heintze[7], H. Heitmann[68], P. Hello[28], G. Hemming[30], M. Hendry[46], I. S. Heng[46], J. Hennig[46], A. W. Heptonstall[1], M. Heurs[10,22], S. Hild[46], T. Hinderer[67], D. Hoak[30], D. Hofman[26], K. Holt[7], D. E. Holz[92], P. Hopkins[36], C. Horst[21], J. Hough[46], E. A. Houston[46], E. J. Howell[66], A. Hreibi[68], Y. M. Hu[10], E. A. Huerta[12], D. Huet[28], B. Hughey[37], S. Husa[102], S. H. Huttner[46], T. Huynh-Dinh[7], N. Indik[10], R. Inta[85], G. Intini[35,98], H. N. Isa[46], J.-M. Isac[72], M. Isi[1], B. R. Iyer[20], K. Izumi[47], T. Jacqmin[72], K. Jani[78], P. Jaranowski[124], S. Jawahar[64], F. Jiménez-Forteza[102], W. W. Johnson[2], D. I. Jones[125], R. Jones[46], R. J. G. Jonker[14], L. Ju[66], J. Junker[10], C. V. Kalaghatgi[36], V. Kalogera[91], B. Kamai[1], S. Kandhasamy[7], G. Kang[40], J. B. Kanner[1], S. J. Kapadia[21], S. Karki[71], K. S. Karvinen[10], M. Kasprzack[2], W. Kastaun[10], M. Katolik[12], E. Katsavounidis[15], W. Katzman[7], S. Kaufer[22], K. Kawabe[47], F. Kéfélian[68], D. Keitel[46], A. J. Kemball[12], R. Kennedy[106], C. Kent[36], J. S. Key[126], F. Y. Khalili[63], I. Khan[17,33], S. Khan[10], Z. Khan[105], E. A. Khazanov[127], N. Kijbunchoo[25], Chunglee Kim[128], J. C. Kim[129], K. Kim[94], W. Kim[74], W. S. Kim[130], Y.-M. Kim[93], S. J. Kimbrell[78], E. J. King[74], P. J. King[47], M. Kinley-Hanlon[123], R. Kirchhoff[10], J. S. Kissel[47], L. Kleybolte[34], S. Klimenko[5], T. D. Knowles[41], P. Koch[10], S. M. Koehlenbeck[10], S. Koley[14], V. Kondrashov[1], A. Kontos[15], M. Korobko[34], W. Z. Korth[1], I. Kowalska[75], D. B. Kozak[1], C. Krämer[10], V. Kringel[10], B. Krishnan[10], A. Królak[131,132], G. Kuehn[10], P. Kumar[111], R. Kumar[105], S. Kumar[20], L. Kuo[89], A. Kutynia[131], S. Kwang[21], B. D. Lackey[38], K. H. Lai[94], M. Landry[47], R. N. Lang[133], J. Lange[59], B. Lantz[51], R. K. Lanza[15], A. Lartaux-Vollard[28], P. D. Lasky[6], M. Laxen[7], A. Lazzarini[1], C. Lazzaro[54], P. Leaci[35,98], S. Leavey[46], C. H. Lee[93], H. K. Lee[134], H. M. Lee[135], H. W. Lee[129], K. Lee[46], J. Lehmann[10], A. Lenon[41], M. Leonardi[96,108], N. Leroy[28], N. Letendre[8], Y. Levin[6], T. G. F. Li[94], S. D. Linker[107], J. Liu[66], R. K. L. Lo[94], N. A. Lockerbie[64], L. T. London[36], J. E. Lord[44], M. Lorenzini[17,18], V. Loriette[136], M. Lormand[7], G. Losurdo[24], J. D. Lough[10], C. O. Lousto[59], G. Lovelace[29], H. Lück[10,22], D. Lumaca[32,33], A. P. Lundgren[10], R. Lynch[15], Y. Ma[48], R. Macas[36], S. Macfoy[27], B. Machenschalk[10], M. MacInnis[15], D. M. Macleod[36], I. Magaña Hernandez[21], F. Magaña-Sandoval[44], L. Magaña Zertuche[44], R. M. Magee[65], E. Majorana[35], I. Maksimovic[136], N. Man[68], V. Mandic[45], V. Mangano[46], G. L. Mansell[25], M. Manske[21,25], M. Mantovani[30], F. Marchesoni[43,52], F. Marion[8], S. Márka[50], Z. Márka[50], C. Markakis[12], A. S. Markosyan[51], A. Markowitz[1], E. Maros[1], A. Marquina[101], F. Martelli[120,121], L. Martellini[68], I. W. Martin[46], R. M. Martin[109], D. V. Martynov[15], K. Mason[15], E. Massera[106], A. Masserot[8], T. J. Massinger[1], M. Masso-Reid[46], S. Mastrogiovanni[35,98], A. Matas[45], F. Matichard[1,15], L. Matone[50], N. Mavalvala[15], N. Mazumder[70], R. McCarthy[47], D. E. McClelland[25], S. McCormick[7], L. McCuller[15], S. C. McGuire[137], G. McIntyre[1], J. McIver[1], D. J. McManus[25], L. McNeill[6], T. McRae[25], S. T. McWilliams[41], D. Meacher[65], G. D. Meadors[10,38], M. Mehmet[10], J. Meidam[14], E. Mejuto-Villa[9], A. Melatos[97], G. Mendell[47], R. A. Mercer[21], E. L. Merilh[47], M. Merzougui[68], S. Meshkov[1], C. Messenger[46], C. Messick[65], R. Metzdorff[72], P. M. Meyers[45], H. Miao[60], C. Michel[26], H. Middleton[60], E. E. Mikhailov[138], L. Milano[4,80], A. L. Miller[5,35,98], B. B. Miller[91], J. Miller[15], M. Millhouse[107], O. Minazzoli[68,139], Y. Minenkov[33], J. Ming[38], C. Mishra[140], S. Mitra[19], V. P. Mitrofanov[63], G. Mitselmakher[5], R. Mittleman[15], D. Moffa[86], A. Moggi[24], K. Mogushi[11], M. Mohan[30], S. R. P. Mohapatra[15], M. Montani[120,121], C. J. Moore[13], D. Moraru[47], G. Moreno[47], S. R. Morriss[103], B. Mours[8], C. M. Mow-Lowry[60], G. Mueller[5], A. W. Muir[36], Arunava Mukherjee[10], D. Mukherjee[21], S. Mukherjee[103], N. Mukund[19], A. Mullavey[7], J. Munch[74], E. A. Muñiz[44], M. Muratore[37], P. G. Murray[46], K. Napier[78], I. Nardecchia[32,33], L. Naticchioni[35,98], R. K. Nayak[141], J. Neilson[107], G. Nelemans[14,67], T. J. N. Nelson[7], M. Nery[10], A. Neunzert[117], L. Nevin[1], J. M. Newport[123], G. Newton[46,162], K. K. Y. Ng[94], T. T. Nguyen[25], D. Nichols[67], A. B. Nielsen[10], S. Nissanke[14,67], A. Nitz[10], A. Noack[10], F. Nocera[30], D. Nolting[7], C. North[36], L. K. Nuttall[36], J. Oberling[47], G. D. O'Dea[107], G. H. Ogin[142], J. J. Oh[130], S. H. Oh[130], F. Ohme[10], M. A. Okada[16], M. Oliver[102], P. Oppermann[10], Richard J. Oram[7], B. O'Reilly[7], R. Ormiston[45], L. F. Ortega[5], R. O'Shaughnessy[59], S. Ossokine[38], D. J. Ottaway[74], H. Overmier[7], B. J. Owen[85], A. E. Pace[65],

J. Page[143], M. A. Page[66], A. Pai[115,144], S. A. Pai[62], J. R. Palamos[71], O. Palashov[127], C. Palomba[35], A. Pal-Singh[34], Howard Pan[89], Huang-Wei Pan[89], B. Pang[48], P. T. H. Pang[94], C. Pankow[91], F. Pannarale[36], B. C. Pant[62], F. Paoletti[24], A. Paoli[30], M. A. Papa[10,21,38], A. Parida[19], W. Parker[7], D. Pascucci[46], A. Pasqualetti[30], R. Passaquieti[23,24], D. Passuello[24], M. Patil[132], B. Patricelli[24,145], B. L. Pearlstone[46], M. Pedraza[1], R. Pedurand[26,146], L. Pekowsky[44], A. Pele[7], S. Penn[147], C. J. Perez[47], A. Perreca[1,96,108], L. M. Perri[91], H. P. Pfeiffer[38,111], M. Phelps[46], K. S. Phukon[19], O. J. Piccinni[35,98], M. Pichot[68], F. Piergiovanni[120,121], V. Pierro[9], G. Pillant[30], L. Pinard[26], I. M. Pinto[9], M. Pirello[47], M. Pitkin[46], M. Poe[21], R. Poggiani[23,24], P. Popolizio[30], E. K. Porter[39], A. Post[10], J. Powell[148], J. Prasad[19], J. W. W. Pratt[37], G. Pratten[102], V. Predoi[36], T. Prestegard[21], M. Prijatelj[10], M. Principe[9], S. Privitera[38], G. A. Prodi[96,108], L. G. Prokhorov[63], O. Puncken[10], M. Punturo[43], P. Puppo[35], M. Pürrer[38], H. Qi[21], V. Quetschke[103], E. A. Quintero[1], R. Quitzow-James[71], F. J. Raab[47], D. S. Rabeling[25], H. Radkins[47], P. Raffai[55], S. Raja[62], C. Rajan[62], B. Rajbhandari[85], M. Rakhmanov[103], K. E. Ramirez[103], A. Ramos-Buades[102], P. Rapagnani[35,98], V. Raymond[38], M. Razzano[23,24], J. Read[29], T. Regimbau[68], L. Rei[61], S. Reid[64], D. H. Reitze[1,5], W. Ren[12], S. D. Reyes[44], F. Ricci[35,98], P. M. Ricker[12], S. Rieger[10], K. Riles[117], M. Rizzo[59], N. A. Robertson[1,46], R. Robie[46], F. Robinet[28], A. Rocchi[33], L. Rolland[8], J. G. Rollins[1], V. J. Roma[71], R. Romano[3,4], C. L. Romel[47], J. H. Romie[7], D. Rosińska[56,149], M. P. Ross[150], S. Rowan[46], A. Rüdiger[10], P. Ruggi[30], G. Rutins[27], K. Ryan[47], S. Sachdev[1], T. Sadecki[47], L. Sadeghian[21], M. Sakellariadou[151], L. Salconi[30], M. Saleem[115], F. Salemi[10], A. Samajdar[141], L. Sammut[6], L. M. Sampson[91], E. J. Sanchez[1], L. E. Sanchez[1], N. Sanchis-Gual[87], V. Sandberg[47], J. R. Sanders[44], N. Sarin[6], B. Sassolas[26], B. S. Sathyaprakash[36,65], P. R. Saulson[44], O. Sauter[117], R. L. Savage[47], A. Sawadsky[34], P. Schale[71], M. Scheel[48], J. Scheuer[91], J. Schmidt[10], P. Schmidt[1,67], R. Schnabel[34], R. M. S. Schofield[71], A. Schönbeck[34], E. Schreiber[10], D. Schuette[10,22], B. W. Schulte[10], B. F. Schutz[10,36], S. G. Schwalbe[37], J. Scott[46], S. M. Scott[25], E. Seidel[12], D. Sellers[7], A. S. Sengupta[152], D. Sentenac[30], V. Sequino[17,32,33], A. Sergeev[127], D. A. Shaddock[25], T. J. Shaffer[47], A. A. Shah[143], M. S. Shahriar[91], M. B. Shaner[107], L. Shao[38], B. Shapiro[51], P. Shawhan[77], A. Sheperd[21], D. H. Shoemaker[15], D. M. Shoemaker[78], K. Siellez[78], X. Siemens[21], M. Sieniawska[56], D. Sigg[47], A. D. Silva[16], L. P. Singer[81], A. Singh[10,22,38], A. Singhal[17,35], A. M. Sintes[102], J. Rana[19], B. J. J. Slagmolen[25], B. Smith[7], J. R. Smith[29], R. J. E. Smith[1,6], S. Somala[153], E. J. Son[130], J. A. Sonnenberg[21], B. Sorazu[46], F. Sorrentino[61], T. Souradeep[19], E. Sowell[85], A. P. Spencer[46], A. K. Srivastava[105], K. Staats[37], A. Staley[50], M. Steinke[10], J. Steinlechner[34,46], S. Steinlechner[34], D. Steinmeyer[10], S. P. Stevenson[60,148], R. Stone[103], D. J. Stops[60], K. A. Strain[46], G. Stratta[120,121], S. E. Strigin[63], A. Strunk[47], R. Sturani[154], A. L. Stuver[7], T. Z. Summerscales[155], L. Sun[97], S. Sunil[105], J. Suresh[19], P. J. Sutton[36], B. L. Swinkels[30], M. J. Szczepańczyk[37], M. Tacca[14], S. C. Tait[46], C. Talbot[6], D. Talukder[71], D. B. Tanner[5], M. Tápai[116], A. Taracchini[38], J. D. Tasson[73], J. A. Taylor[143], R. Taylor[1], S. V. Tewari[147], T. Theeg[10], F. Thies[10], E. G. Thomas[60], M. Thomas[7], P. Thomas[47], K. A. Thorne[7], E. Thrane[6], S. Tiwari[17,96], V. Tiwari[36], K. V. Tokmakov[64], K. Toland[46], M. Tonelli[23,24], Z. Tornasi[46], A. Torres-Forné[87], C. I. Torrie[1], D. Töyrä[60], F. Travasso[30,43], G. Traylor[7], J. Trinastic[5], M. C. Tringali[96,108], L. Trozzo[24,156], K. W. Tsang[14], M. Tse[15], R. Tso[1], L. Tsukada[83], D. Tsuna[83], D. Tuyenbayev[103], K. Ueno[21], D. Ugolini[157], C. S. Unnikrishnan[118], A. L. Urban[1], S. A. Usman[36], H. Vahlbruch[22], G. Vajente[1], G. Valdes[2], N. van Bakel[14], M. van Beuzekom[14], J. F. J. van den Brand[14,76], C. Van Den Broeck[14,158], D. C. Vander-Hyde[44], L. van der Schaaf[14], J. V. van Heijningen[14], A. A. van Veggel[46], M. Vardaro[53,54], V. Varma[48], S. Vass[1], M. Vasúth[49], A. Vecchio[60], G. Vedovato[54], J. Veitch[46], P. J. Veitch[74], K. Venkateswara[150], G. Venugopalan[1], D. Verkindt[8], F. Vetrano[120,121], A. Viceré[120,121], A. D. Viets[21], S. Vinciguerra[60], D. J. Vine[27], J.-Y. Vinet[68], S. Vitale[15], T. Vo[44], H. Vocca[42,43], C. Vorvick[47], S. P. Vyatchanin[63], A. R. Wade[1], L. E. Wade[86], M. Wade[86], R. Walet[14], M. Walker[29], L. Wallace[1], S. Walsh[10,21,38], G. Wang[17,121], H. Wang[60], J. Z. Wang[65], W. H. Wang[103], Y. F. Wang[94], R. L. Ward[25], J. Warner[47], M. Was[8], J. Watchi[99], B. Weaver[47], L.-W. Wei[10,22], M. Weinert[10], A. J. Weinstein[1], R. Weiss[15], L. Wen[66], E. K. Wessel[12], P. Weßels[10], J. Westerweck[10], T. Westphal[10], K. Wette[25], J. T. Whelan[59], D. D. White[29], B. F. Whiting[5], C. Whittle[6], D. Wilken[10], D. Williams[46], R. D. Williams[1], A. R. Williamson[67], J. L. Willis[1,159], B. Willke[10,22], M. H. Wimmer[10], W. Winkler[10], C. C. Wipf[1], H. Wittel[10,22], G. Woan[46], J. Woehler[10], J. Wofford[59], K. W. K. Wong[94], J. Worden[47], J. L. Wright[46], D. S. Wu[10], D. M. Wysocki[59], S. Xiao[1], H. Yamamoto[1], C. C. Yancey[77], L. Yang[160], M. J. Yap[25], M. Yazback[5], Hang Yu[15], Haocun Yu[15], M. Yvert[8], A. Zadrożny[131], M. Zanolin[37], T. Zelenova[30], J.-P. Zendri[54], M. Zevin[91], L. Zhang[1], M. Zhang[138], T. Zhang[46], Y.-H. Zhang[59], C. Zhao[66], M. Zhou[91], Z. Zhou[91], S. J. Zhu[10,38], X. J. Zhu[6], A. B. Zimmerman[111], M. E. Zucker[1,15], and J. Zweizig[1],

(LIGO Scientific Collaboration and Virgo Collaboration)

[1] LIGO, California Institute of Technology, Pasadena, CA 91125, USA
[2] Louisiana State University, Baton Rouge, LA 70803, USA
[3] Università di Salerno, Fisciano, I-84084 Salerno, Italy
[4] INFN, Sezione di Napoli, Complesso Universitario di Monte S.Angelo, I-80126 Napoli, Italy
[5] University of Florida, Gainesville, FL 32611, USA
[6] OzGrav, School of Physics & Astronomy, Monash University, Clayton, VIC 3800, Australia
[7] LIGO Livingston Observatory, Livingston, LA 70754, USA
[8] Laboratoire d'Annecy-le-Vieux de Physique des Particules (LAPP), Université Savoie Mont Blanc, CNRS/IN2P3, F-74941 Annecy, France
[9] University of Sannio at Benevento, I-82100 Benevento, Italy and INFN, Sezione di Napoli, I-80100 Napoli, Italy
[10] Max Planck Institute for Gravitational Physics (Albert Einstein Institute), D-30167 Hannover, Germany
[11] The University of Mississippi, University, MS 38677, USA
[12] NCSA, University of Illinois at Urbana-Champaign, Urbana, IL 61801, USA

[13] University of Cambridge, Cambridge CB2 1TN, UK

[14] Nikhef, Science Park, 1098 XG Amsterdam, The Netherlands

[15] LIGO, Massachusetts Institute of Technology, Cambridge, MA 02139, USA

[16] Instituto Nacional de Pesquisas Espaciais, 12227-010 São José dos Campos, São Paulo, Brazil

[17] Gran Sasso Science Institute (GSSI), I-67100 L'Aquila, Italy

[18] INFN, Laboratori Nazionali del Gran Sasso, I-67100 Assergi, Italy

[19] Inter-University Centre for Astronomy and Astrophysics, Pune 411007, India

[20] International Centre for Theoretical Sciences, Tata Institute of Fundamental Research, Bengaluru 560089, India

[21] University of Wisconsin-Milwaukee, Milwaukee, WI 53201, USA

[22] Leibniz Universität Hannover, D-30167 Hannover, Germany

[23] Università di Pisa, I-56127 Pisa, Italy

[24] INFN, Sezione di Pisa, I-56127 Pisa, Italy

[25] OzGrav, Australian National University, Canberra, ACT 0200, Australia

[26] Laboratoire des Matériaux Avancés (LMA), CNRS/IN2P3, F-69622 Villeurbanne, France

[27] SUPA, University of the West of Scotland, Paisley PA1 2BE, UK

[28] LAL, Univ. Paris-Sud, CNRS/IN2P3, Université Paris-Saclay, F-91898 Orsay, France

[29] California State University Fullerton, Fullerton, CA 92831, USA

[30] European Gravitational Observatory (EGO), I-56021 Cascina, Pisa, Italy

[31] Chennai Mathematical Institute, Chennai 603103, India

[32] Università di Roma Tor Vergata, I-00133 Roma, Italy

[33] INFN, Sezione di Roma Tor Vergata, I-00133 Roma, Italy

[34] Universität Hamburg, D-22761 Hamburg, Germany

[35] INFN, Sezione di Roma, I-00185 Roma, Italy

[36] Cardiff University, Cardiff CF24 3AA, UK

[37] Embry-Riddle Aeronautical University, Prescott, AZ 86301, USA

[38] Max Planck Institute for Gravitational Physics (Albert Einstein Institute), D-14476 Potsdam-Golm, Germany

[39] APC, AstroParticule et Cosmologie, Université Paris Diderot, CNRS/IN2P3, CEA/Irfu, Observatoire de Paris, Sorbonne Paris Cité,
F-75205 Paris Cedex 13, France

[40] Korea Institute of Science and Technology Information, Daejeon 34141, Korea

[41] West Virginia University, Morgantown, WV 26506, USA

[42] Università di Perugia, I-06123 Perugia, Italy

[43] INFN, Sezione di Perugia, I-06123 Perugia, Italy

[44] Syracuse University, Syracuse, NY 13244, USA

[45] University of Minnesota, Minneapolis, MN 55455, USA

[46] SUPA, University of Glasgow, Glasgow G12 8QQ, UK

[47] LIGO Hanford Observatory, Richland, WA 99352, USA

[48] Caltech CaRT, Pasadena, CA 91125, USA

[49] Wigner RCP, RMKI, H-1121 Budapest, Konkoly Thege Miklós út 29-33, Hungary

[50] Columbia University, New York, NY 10027, USA

[51] Stanford University, Stanford, CA 94305, USA

[52] Università di Camerino, Dipartimento di Fisica, I-62032 Camerino, Italy

[53] Università di Padova, Dipartimento di Fisica e Astronomia, I-35131 Padova, Italy

[54] INFN, Sezione di Padova, I-35131 Padova, Italy

[55] Institute of Physics, Eötvös University, Pázmány P.s. 1/A, Budapest 1117, Hungary

[56] Nicolaus Copernicus Astronomical Center, Polish Academy of Sciences, 00-716 Warsaw, Poland

[57] Dipartimento di Scienze Matematiche, Fisiche e Informatiche, Università di Parma, I-43124 Parma, Italy

[58] INFN, Sezione di Milano Bicocca, Gruppo Collegato di Parma, I-43124 Parma, Italy

[59] Rochester Institute of Technology, Rochester, NY 14623, USA

[60] University of Birmingham, Birmingham B15 2TT, UK

[61] INFN, Sezione di Genova, I-16146 Genova, Italy

[62] RRCAT, Indore MP 452013, India

[63] Faculty of Physics, Lomonosov Moscow State University, Moscow 119991, Russia

[64] SUPA, University of Strathclyde, Glasgow G1 1XQ, UK

[65] The Pennsylvania State University, University Park, PA 16802, USA

[66] OzGrav, University of Western Australia, Crawley, WA 6009, Australia

[67] Department of Astrophysics/IMAPP, Radboud University Nijmegen, P.O. Box 9010, 6500 GL Nijmegen, The Netherlands

[68] Artemis, Université Côte d'Azur, Observatoire Côte d'Azur, CNRS, CS 34229, F-06304 Nice Cedex 4, France

[69] Institut FOTON, CNRS, Université de Rennes 1, F-35042 Rennes, France

[70] Washington State University, Pullman, WA 99164, USA

[71] University of Oregon, Eugene, OR 97403, USA

[72] Laboratoire Kastler Brossel, UPMC-Sorbonne Universités, CNRS, ENS-PSL Research University, Collège de France, F-75005 Paris, France

[73] Carleton College, Northfield, MN 55057, USA

[74] OzGrav, University of Adelaide, Adelaide, SA 5005, Australia

[75] Astronomical Observatory Warsaw University, 00-478 Warsaw, Poland

[76] VU University Amsterdam, 1081 HV Amsterdam, The Netherlands

[77] University of Maryland, College Park, MD 20742, USA

[78] Center for Relativistic Astrophysics, Georgia Institute of Technology, Atlanta, GA 30332, USA

[79] Université Claude Bernard Lyon 1, F-69622 Villeurbanne, France

[80] Università di Napoli "Federico II," Complesso Universitario di Monte S.Angelo, I-80126 Napoli, Italy

[81] NASA Goddard Space Flight Center, Greenbelt, MD 20771, USA

[82] Dipartimento di Fisica, Università degli Studi di Genova, I-16146 Genova, Italy

[83] RESCEU, University of Tokyo, Tokyo, 113-0033, Japan

[84] Tsinghua University, Beijing 100084, China

[85] Texas Tech University, Lubbock, TX 79409, USA

[86] Kenyon College, Gambier, OH 43022, USA

[87] Departamento de Astronomía y Astrofísica, Universitat de València, E-46100 Burjassot, València, Spain
[88] Museo Storico della Fisica e Centro Studi e Ricerche Enrico Fermi, I-00184 Roma, Italy
[89] National Tsing Hua University, Hsinchu City, 30013 Taiwan, China
[90] Charles Sturt University, Wagga Wagga, NSW 2678, Australia
[91] Center for Interdisciplinary Exploration & Research in Astrophysics (CIER.A.), Northwestern University, Evanston, IL 60208, USA
[92] University of Chicago, Chicago, IL 60637, USA
[93] Pusan National University, Busan 46241, Korea
[94] The Chinese University of Hong Kong, Shatin, NT, Hong Kong
[95] INAF, Osservatorio Astronomico di Padova, I-35122 Padova, Italy
[96] INFN, Trento Institute for Fundamental Physics and Applications, I-38123 Povo, Trento, Italy
[97] OzGrav, University of Melbourne, Parkville, VIC 3010, Australia
[98] Università di Roma "La Sapienza," I-00185 Roma, Italy
[99] Université Libre de Bruxelles, Brussels B-1050, Belgium
[100] Sonoma State University, Rohnert Park, CA 94928, USA
[101] Departamento de Matemáticas, Universitat de València, E-46100 Burjassot, València, Spain
[102] Universitat de les Illes Balears, IAC3—IEEC, E-07122 Palma de Mallorca, Spain
[103] The University of Texas Rio Grande Valley, Brownsville, TX 78520, USA
[104] Bellevue College, Bellevue, WA 98007, USA
[105] Institute for Plasma Research, Bhat, Gandhinagar 382428, India
[106] The University of Sheffield, Sheffield S10 2TN, UK
[107] California State University, Los Angeles, 5151 State University Drive, Los Angeles, CA 90032, USA
[108] Università di Trento, Dipartimento di Fisica, I-38123 Povo, Trento, Italy
[109] Montclair State University, Montclair, NJ 07043, USA
[110] National Astronomical Observatory of Japan, 2-21-1 Osawa, Mitaka, Tokyo 181-8588, Japan
[111] Canadian Institute for Theoretical Astrophysics, University of Toronto, Toronto, ON M5S 3H8, Canada
[112] Observatori Astronòmic, Universitat de València, E-46980 Paterna, València, Spain
[113] School of Mathematics, University of Edinburgh, Edinburgh EH9 3FD, UK
[114] University and Institute of Advanced Research, Koba Institutional Area, Gandhinagar Gujarat 382007, India
[115] IISER-TVM, CET Campus, Trivandrum Kerala 695016, India
[116] University of Szeged, Dóm tér 9, Szeged 6720, Hungary
[117] University of Michigan, Ann Arbor, MI 48109, USA
[118] Tata Institute of Fundamental Research, Mumbai 400005, India
[119] INAF, Osservatorio Astronomico di Capodimonte, I-80131, Napoli, Italy
[120] Università degli Studi di Urbino "Carlo Bo," I-61029 Urbino, Italy
[121] INFN, Sezione di Firenze, I-50019 Sesto Fiorentino, Firenze, Italy
[122] Physik-Institut, University of Zurich, Winterthurerstrasse 190, 8057 Zurich, Switzerland
[123] American University, Washington, DC 20016, USA
[124] University of Białystok, 15-424 Białystok, Poland
[125] University of Southampton, Southampton SO17 1BJ, UK
[126] University of Washington Bothell, 18115 Campus Way NE, Bothell, WA 98011, USA
[127] Institute of Applied Physics, Nizhny Novgorod, 603950, Russia
[128] Korea Astronomy and Space Science Institute, Daejeon 34055, Korea
[129] Inje University Gimhae, South Gyeongsang 50834, Korea
[130] National Institute for Mathematical Sciences, Daejeon 34047, Korea
[131] NCBJ, 05-400 Świerk-Otwock, Poland
[132] Institute of Mathematics, Polish Academy of Sciences, 00656 Warsaw, Poland
[133] Hillsdale College, Hillsdale, MI 49242, USA
[134] Hanyang University, Seoul 04763, Korea
[135] Seoul National University, Seoul 08826, Korea
[136] ESPCI, CNRS, F-75005 Paris, France
[137] Southern University and A&M College, Baton Rouge, LA 70813, USA
[138] College of William and Mary, Williamsburg, VA 23187, USA
[139] Centre Scientifique de Monaco, 8 quai Antoine Ier, MC-98000, Monaco
[140] Indian Institute of Technology Madras, Chennai 600036, India
[141] IISER-Kolkata, Mohanpur, West Bengal 741252, India
[142] Whitman College, 345 Boyer Avenue, Walla Walla, WA 99362 USA
[143] NASA Marshall Space Flight Center, Huntsville, AL 35811, USA
[144] Indian Institute of Technology Bombay, Powai, Mumbai, Maharashtra 400076, India
[145] Scuola Normale Superiore, Piazza dei Cavalieri 7, I-56126 Pisa, Italy
[146] Université de Lyon, F-69361 Lyon, France
[147] Hobart and William Smith Colleges, Geneva, NY 14456, USA
[148] OzGrav, Swinburne University of Technology, Hawthorn, VIC 3122, Australia
[149] Janusz Gil Institute of Astronomy, University of Zielona Góra, 65-265 Zielona Góra, Poland
[150] University of Washington, Seattle, WA 98195, USA
[151] King's College London, University of London, London WC2R 2LS, UK
[152] Indian Institute of Technology, Gandhinagar Ahmedabad Gujarat 382424, India
[153] Indian Institute of Technology Hyderabad, Sangareddy, Khandi, Telangana 502285, India
[154] International Institute of Physics, Universidade Federal do Rio Grande do Norte, Natal RN 59078-970, Brazil
[155] Andrews University, Berrien Springs, MI 49104, USA
[156] Università di Siena, I-53100 Siena, Italy
[157] Trinity University, San Antonio, TX 78212, USA
[158] Van Swinderen Institute for Particle Physics and Gravity, University of Groningen, Nijenborgh 4, 9747 AG Groningen, The Netherlands
[159] Abilene Christian University, Abilene, TX 79699, USA
[160] Colorado State University, Fort Collins, CO 80523, USA
[161] Deceased, 2017 February.
[162] Deceased, 2016 December.